https://doi.org/10.5194/egusphere-2026-6695
Preprint. Discussion started: 5 November 2026
© Author(s) 2026. CC BY 4.0 License.

Hydrogen chloride formation from mixed inorganic aerosols revealed by in-flight X-ray photoelectron spectroscopy

Calle Preger[1,2,3], Axel C. Eriksson[2,3], Jack J. Lin[4], Noelle Walsh[1], Antti Kivimäki[1], Nønne L. Prisle[4,5,6,7], Birgitta Svenningsson[7], and Jenny Rissler[2,3]

[1]MAX IV Laboratory, Lund University, SE-22100 Lund, Sweden
[2]Ergonomics and Aerosol Technology, Lund University, SE-22100 Lund, Sweden,
[3]NanoLund, Lund University, SE-22100 Lund, Sweden
[4]Centre for Atmospheric Research, University of Oulu, PO BOX 4500, FI-90014 Oulu, Finland
[5]Centre for Molecular Water Science (CMWS), Deutsches Elektronen-Synchrotron DESY, Notkestraße 85, D-22607 Hamburg, Germany
[6]Institute of Inorganic and Applied Chemistry, University of Hamburg, Martin-Luther-King-Platz 6, D-20146 Hamburg, Germany
[7]Physics Department, Lund University, SE-22100 Lund, Sweden

Correspondence to: Jenny Rissler (jenny.rissler@design.lth.se)

Abstract. Understanding the physicochemical properties of inorganic aerosol mixtures is important for accurately predicting their atmospheric behavior and climate impacts. Here, we apply in-flight X-ray photoelectron spectroscopy (XPS) to study particle- and gas-phase chlorine in aerosols generated from nebulized mixed NaCl and $(NH_4)_2SO_4$ solutions. By detecting Cl 2p photoelectrons from the particle surface and gas-phase hydrogen chloride (HCl), we provide experimental evidence of gaseous HCl formation during aerosol generation and drying. The dual-phase capability of the in-flight XPS approach enables clear identification of how relative humidity (RH) and aerosol mass concentration influence Cl gas-particle partitioning. We demonstrate that HCl formation is strongly dependent on the RH after drying, with increasing HCl evaporation as the RH decreases from 40% to 10%, while the extent of HCl formation remains largely independent of the aerosol mass concentration within the range 1700 µg/m³ - 6500 µg/m³. The results provide direct confirmation of key processes governing HCl partitioning in mixed inorganic aerosols and contribute to a better understanding of aerosol chemistry, relevant for atmospheric modeling and climate prediction. These findings further demonstrate the power of combining intense synchrotron radiation, XPS, and an in-flight aerosol sample-delivery system.

1. Introduction

Atmospheric aerosols are generated through a wide range of natural and anthropogenic processes. The sources of aerosols are diverse and so too are their composition, often consisting of complex mixtures of organic and inorganic components, trace metals, in various mixing states and chemical forms.

In the atmosphere, aerosol particles play a crucial role through their interaction with water vapor, contributing to the formation of cloud and fog droplets, and ice crystals. These interactions significantly influence Earth's radiation balance (e.g., global

https://doi.org/10.5194/egusphere-2026-6695
Preprint. Discussion started: 5 November 2026
© Author(s) 2026. CC BY 4.0 License.

climate) (Calvin et al., 2023) and affect both global and regional hydrological systems (Ramanathan et al., 2001). Furthermore, aerosol particles are essential to atmospheric chemistry, participating in numerous chemical transformations (Andreae and Crutzen, 1997; Li and Kuwata, 2023).

Understanding the chemistry of aerosol particles is necessary for accurately modeling and predicting their atmospheric residence time, transport of pollutants, and impact on global climate (George and Abbatt, 2010). The interactions between various components in the atmosphere, between particles and gas-phase species, and effect on cloud nucleation are highly complex and remain an active area of research (Prisle, 2024; Zieger et al., 2017).

As the particle water uptake and chemistry of inorganic mixtures is considered generally well understood, any deviations from expected outcomes have often been attributed to the less understood effects of organic components (Hallquist et al., 2009; Prisle et al., 2010). However, in a previous study, involving the nebulization and drying of solutions containing four prevalent atmospheric ions: Na^+, Cl^-, NH_4^+, and SO_4^{2-}, we provided evidence that the evaporation of HCl and NH_3 during drying of droplets can, under commonly occurring conditions, significantly alter the chemical composition of the dried particles (Rissler et al., 2023). The evaporation is expected to be most pronounced when the particles exist as supersaturated salt solutions.

Neglecting such losses of the solute to the gas phase may result in erroneous interpretation of, for example, laboratory experiments of particle water uptake. The impact of evaporation on particle water uptake is most pronounced for particles containing both hygroscopic inorganic components and less hygroscopic substances, such as high molecular weight organics. This is because, as inorganic ions are lost, the relative share of less hygroscopic organic material increases which reduces the overall particle hygroscopicity (Rissler et al., 2023; Svenningsson et al., 2006). Similarly, Gorai et al., 2014, studied the hygroscopic properties of laboratory generated NaCl particles mixed with malonic acid and glutaric acid attributed the depletion of chloride to the HCl evaporation from dehydrating particles. Detailed thermodynamic models, such as the E-AIM model, predict the evaporation of certain inorganic species (Clegg et al., 1998). However, evaporation of inorganic species is rarely acknowledged or accounted for in practice, although it typically occurs at aerosol mass concentrations commonly used in lab experiments. In droplets containing Na^+, Cl^-, NH_4^+, and SO_4^{2-}, gas-particle partitioning depends on aerosol mass concentration in the system, and the evaporation becomes most evident at low concentrations typically relevant for atmospheric conditions. E-AIM further predicts a dependence of the evaporation on relative humidity (RH), with HCl evaporation from droplets becoming more pronounced at lower RH (Rissler et al., 2023). The evidence for the evaporation of components to the gas phase presented by Rissler et al. (2023) was concluded from observations of alterations between measured and model-predicted particle hygroscopic growth, and a concentration-dependent shift in the molar ratio of NH_4^+ to SO_4^{2-} in the particle phase, but no gaseous components were confirmed.

Here, we present direct observations of particle surface and gas-phase chlorides, confirming HCl formation and its dependence on RH and aerosol mass concentration during drying of droplets from nebulized solutions of NaCl mixed with $(NH_4)_2SO_4$. It was investigated using an aerosol sample-delivery system (ASDS) designed for in-flight X-ray Photoelectron Spectroscopy (XPS) measurements on aerosols (Preger et al., 2024). In-flight XPS has previously been employed to examine surface enrichment in salt mixtures (Antonsson et al., 2015; Kong et al., 2025; Pelimanni et al., 2022), organic mixtures (Deal et al.,

https://doi.org/10.5194/egusphere-2026-6695
Preprint. Discussion started: 5 November 2026
© Author(s) 2026. CC BY 4.0 License.

2025), and the influence of organic components on the surface composition of inorganic mixtures (Unger et al., 2020). The set-up also allows in-situ studies of particle and gas-phase simultaneously, such as Cl at particle surface and in the gas-phase. The surface and gas contributions are well separated in the XPS spectrum due to the large relative shift in binding energy, which allows us to assess HCl release under varying aerosol mass concentrations and RH.

2. Methods

2.1 Aerosol generation

NaCl and $(NH_4)_2SO_4$ were mixed in MilliQ-water in molar ratios of 2:1, resulting in an ion molar ratio of 1:1:1:0.5 (Na^+:Cl^-:NH_4^+:SO_4^{2-}) in the solution. Three solutions, all with the same ion molar ratio, were prepared with different total concentrations of the salt in the mixture: 1, 0.5, and 0.25 g/l. The salt solutions were nebulized using a constant output atomizer (TSI model 3076) with N_2 as the carrier gas. The aerosol passed through two diffusion dryers (TSI 3062-NC and TOPAS DDU 570/H) before it entered the ASDS. The RH of the aerosol after the drying was varied by different water content in the silica gel and continuously monitored using an RH monitor (VelociCalc Model 9565). The particle number size distribution of the dried particles was measured in parallel using a Scanning Mobility Particle Sizer (SMPS, TSI 3082).

2.2. X-ray photoelectron spectroscopy

The ASDS (Preger et al., 2024) was utilized at the gas-phase end station (GPES) (Kooser et al., 2020) of the FinEstBeAMS beamline (Chernenko et al., 2021) at MAX IV Laboratory, Lund, Sweden. The ASDS operates by continuously transporting aerosol particles and gas molecules from atmospheric pressure to a measurement chamber under high vacuum (10^{-6} mbar with aerosol load) for in-flight XPS measurements.

Using the in-flight system, the aerosol being sampled is continuously renewed, which minimizes the risk of beam damage and charge buildup (Preger et al., 2024). Furthermore, it lowers the risk of oxidation or other surface alteration that may occur between the sample preparation (e.g., generation and deposition onto a substrate) and measurement. A prominent feature of the ASDS is that it enables simultaneous XPS measurements of particle surfaces along with the gas phase accompanying the particles during the process of aerosol generation.

The aerosol pathway from nebulization to XPS measurement is depicted schematically in Figure 1. The aerosol was introduced to the ASDS through a 140 µm critical orifice, resulting in a constant aerosol flow rate of 0.18 lpm (at atmospheric pressure) into the ASDS. The excess aerosol flow was either led to the SMPS or released to an exhaust line. The aerosol entering the ASDS flows through a relaxation tube before being transmitted through an aerodynamic lens (Aerodyne PM1) (Liu et al., 1995). The aerodynamic lens consists of a series of orifices that collimate and form a narrow beam of particles in the aerosol. The orifice dimensions in the aerodynamic lens are described in detail by Zhang et al. (2004). After the aerodynamic lens, the collimated aerosol particle beam passes through a 1.5 mm conical skimmer separating the ASDS chamber from the GPES

https://doi.org/10.5194/egusphere-2026-6695
Preprint. Discussion started: 5 November 2026
© Author(s) 2026. CC BY 4.0 License.

chamber at FinEstBeAMS. In this step, most gas molecules are skimmed away, reducing the pressure from 10^{-3} mbar range in the ASDS chamber to 10^{-6} mbar range in the GPES chamber, while the aerosol particles continue to travel as a narrow beam with minimal losses. In the GPES chamber, the narrow aerosol particle beam and gas molecules cross the photon beam. As a result of the interaction between the aerosol and the photon beam, electrons are emitted. Some of these electrons are emitted in the directions of the entrance to the SCIENTA R4000 electron analyzer, where their kinetic energies are analyzed.

When the ASDS is coupled to the GPES, the electron analyzer of the GPES is positioned vertically to the incoming photon beam. To maximize photoelectron signal intensity in the direction of the electron analyzer, the radiation source of the beamline, an elliptically polarizing undulator, was set to provide light with vertical linear polarization. The Cl 2p photoelectron spectra were measured at 273 eV photon energy. The photon energy was chosen such that the kinetic energies of the detected photoelectrons would be about 70 eV to achieve high surface specific measurement sensitivity. All spectra were recorded using a 300 µm exit slit for the beamline, as well as 100 eV pass energy and a 1.5 mm straight slit for the electron analyzer, providing a total instrumental resolution of approximately 500 meV. The energy scale was calibrated using the Cl $2p_{3/2}$ feature of the HCl gas molecules. The Cl $2p_{3/2}$ feature consists of two close-lying components arising from molecular-field splitting, which are not resolved here. The average binding energy of the two components, 207.4 eV, was used for energy calibration (Ellingsen et al., 1997).

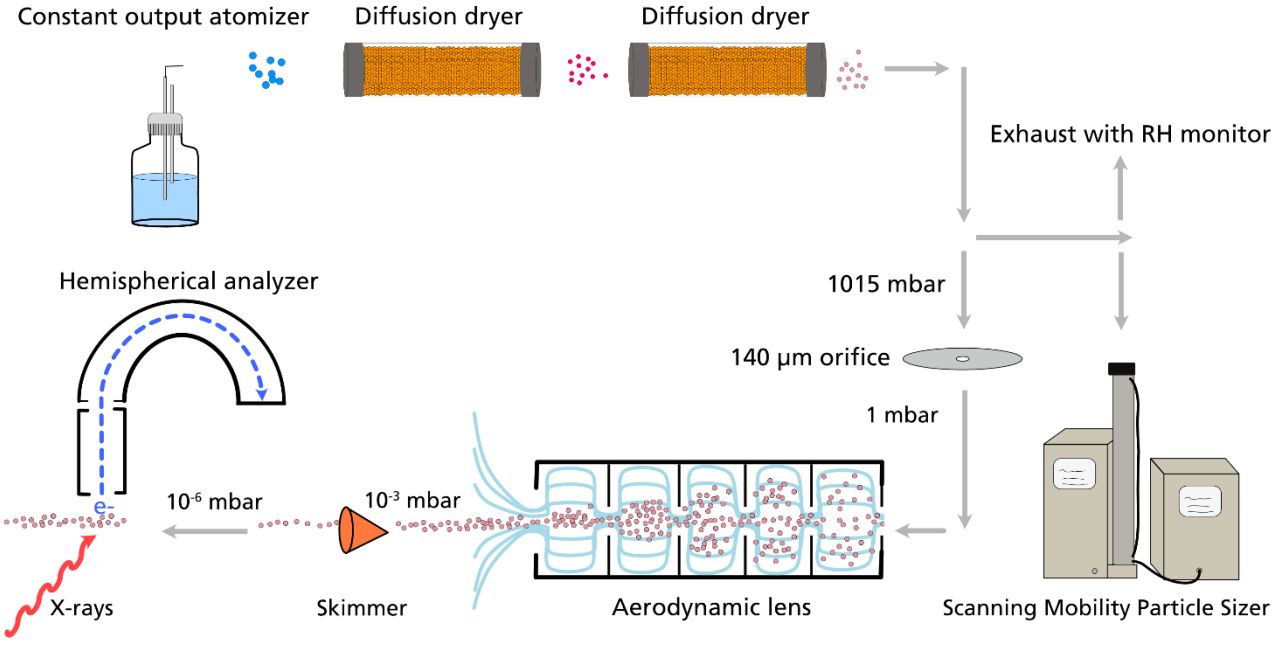


Figure 1: Experimental setup. The salt solutions were aerosolized by a constant output atomizer, and the droplets were dried in two diffusion dryers. The aerosol was directed to i) an SMPS to monitor the particle number size distribution, ii) to an exhaust line with an RH monitor, and iii) to the ASDS for in-flight XPS measurements. The aerosol enters the

https://doi.org/10.5194/egusphere-2026-6695
Preprint. Discussion started: 5 November 2026
© Author(s) 2026. CC BY 4.0 License.

ASDS through a 140 µm critical orifice before the aerosol particle beam is collimated and narrowed by an aerodynamic lens. The interaction with the photon beam takes place in a vacuum chamber separated from the aerodynamic lens chamber by a conical skimmer.

2.2. Thermodynamic modeling using E-AIM

The thermodynamic equilibrium model E-AIM (http://www.aim.env.uea.ac.uk/aim/aim.php, Model III, Clegg et al. 1998) was used to evaluate the gas-phase/aqueous-phase partitioning. The concentrations modeled (in moles solute per cubic meter of air) were in a range that corresponded to the aerosol mass concentrations used in the XPS measurements, estimated from the SMPS data. The three concentrations of the ions modeled (Na^+; Cl^-; NH_4^+; SO_4^{2-}) were (1.34; 1.34; 1.34; 0.67)·10^{-5} mole/m^3, (2.42; 2.42; 2.42; 1.21)·10^{-5} mole/m^3, and (5.17; 5.17; 5.17; 2.59)·10^{-5} mole/m^3. These concentrations correspond to the aerosol mass concentrations of 1660, 3020, and 6450 µg/m^3, respectively. To be able to model the efflorescence branch of the hygroscopic growth curve, no crystal forms were allowed. The efflorescence branch corresponds to supersaturated solutions being formed during the drying of the solution droplets. E-AIM only models the bulk chemistry and the gas phase, while the surface-bulk partitioning of ionic compounds is not considered.

3. Results

3.1. Aerosol particle generation

The aerosols generated from solutions of different concentrations (1, 0.5, 0.25 g/l) and at 40% RH were analyzed with the SMPS. The three concentrations showed a noticeable shift in dry particle mobility size distribution (Figure 2a). As expected, both the total particle mass concentration and the geometric mean particle diameter decreased with lowered salt concentration in the solutions (Figure 2b-c). The surface weighted size distributions, also shown alongside with number size distributions in Figure 2a, provide a relative measure of cross section between the particles and the photon beam during the XPS measurements. For the surface weighted geometric mean diameter of the distributions, the reduction in size was from 114 nm to 83 nm (Figure 2b, squares), which falls well within the range where the transmission efficiency in the aerodynamic lens is above 90% (Liu et al., 2007). Assuming spherical particles with a dry density of 2.00 g/cm³ (for comparison, densities of NaCl: 2.16 g/cm3, Na_2SO_4: 2.66 g/cm^3, NH_4Cl: 1.53 g/cm^3, $(NH_4)_2SO_4$: 1.77 g/cm^3), the resulting aerosol mass concentration obtained from SMPS was estimated to range between 1660 µg/m³ and 6450 µg/m³ (Figure 2c, diamonds).

https://doi.org/10.5194/egusphere-2026-6695
Preprint. Discussion started: 5 November 2026
© Author(s) 2026. CC BY 4.0 License.

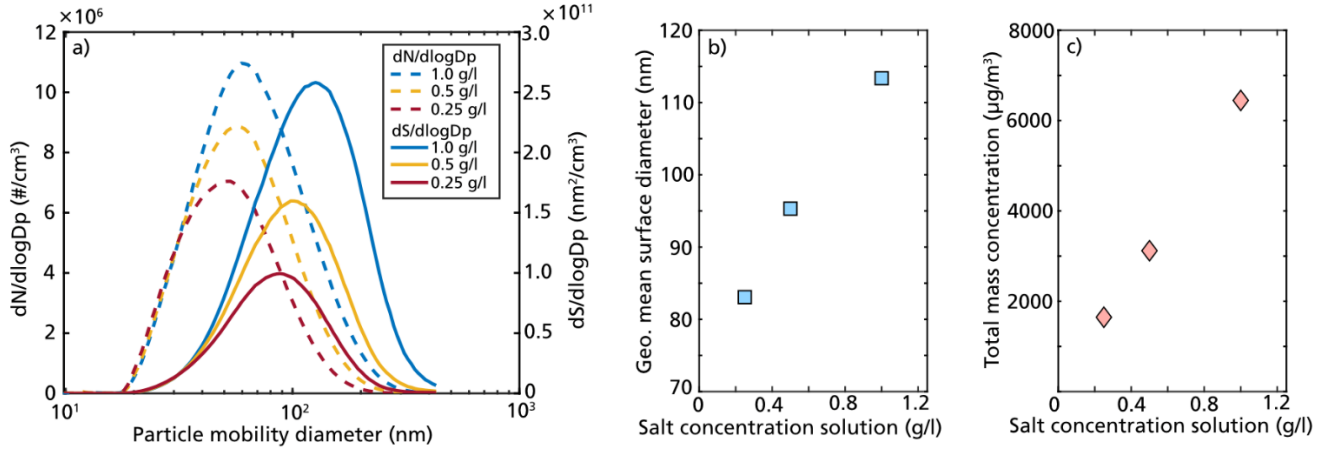


Figure 2: (a) Particle mobility size distributions of salt solutions at different mass concentrations (left panel). The dashed lines are the number size distributions (dN/dlogDp), and the solid lines are the weighted surface concentrations (dS/dlogDp) which assume spherical particles. In panel b and c, the surface weighted geometric mean diameter (b, blue square) and the total mass concentration (c, red diamond) are plotted against the salt concentration in the solution.

3.2. Gas-particle partitioning

Figure 3 presents the Cl 2p photoelectron spectra of aerosols generated with different aerosol mass concentrations and different RH, with black lines indicating the results from peak fitting. RH refers to that measured in the aerosol flow after the dryers. Each spectrum contains four peaks arising from two pairs of spin-orbit-split Cl 2p doublets. In the analysis of the spectra, each doublet was fitted with the characteristic 2:1 area ratio and a fixed spin-orbit-splitting of 1.6 eV (Barrie et al., 1974). The doublet at lower binding energy (202-205 eV) is attributed to the Cl signal from the particle surface and the doublet at higher binding energy (207-210 eV) is attributed to hydrogen chloride (HCl) gaseous molecules (Kivilompolo et al., 2000). The full width at half maximum (FWHM) of the fitted peaks was set to 1.15 eV (±0.05 eV) for the Cl (particle) doublet and 0.57 eV (±0.05 eV) for the HCl gas molecule doublet. All spectra have been normalized to the measurement time, thus the signal intensities of the spectra are intercomparable.

https://doi.org/10.5194/egusphere-2026-6695
Preprint. Discussion started: 5 November 2026
© Author(s) 2026. CC BY 4.0 License.

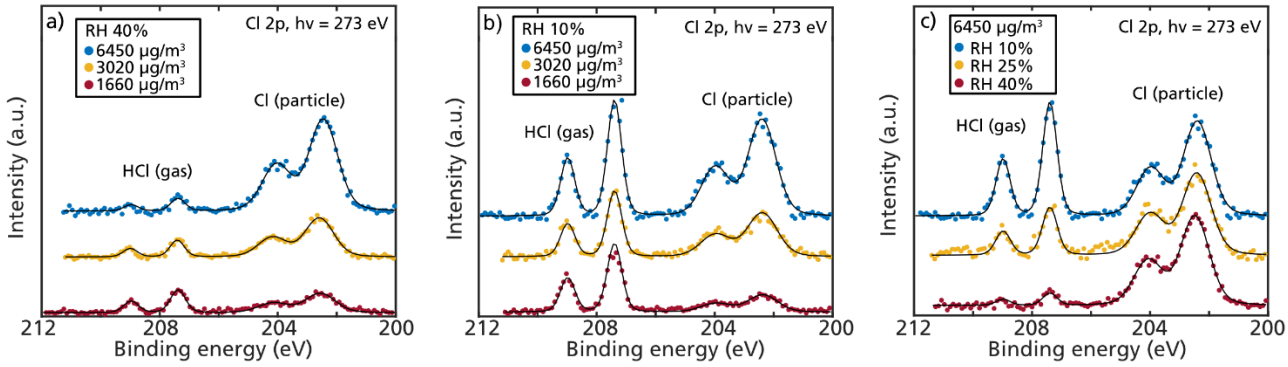


Figure 3: Cl 2p photoelectron spectra. Panels a) and b) show the Cl 2p particle and HCl gas signal with different aerosol mass concentrations at a fixed RH (40% and 10%). In c) the aerosol mass concentration is fixed (6450 µg/m3) and RH changes. By lowering the aerosol mass concentration while keeping the RH fixed, the particle signal decreases, while minor changes are observed for the gas signal (a-b). In contrast when lowering the RH but keeping mass concentration fixed, the HCl (g) signal clearly increases, and the particle signal appears unchanged (c).

Figure 3 shows how the relative signal intensities from Cl 2p in the particles and the gas phase change with the aerosol mass concentration and RH. Figure 3a shows how the photoelectron signal of the Cl from the particles measured at 40% RH decreases with lowered mass concentration while the HCl (g) remains low and nearly unaffected at the different mass concentrations. Figure 3b shows the same as in Figure 3a but at a lower RH, in this case 10%. The main difference in the photoelectron spectra between the high (40%) and low (10%) RH is the intensified HCl (g) signal at low RH. Figure 3c displays how the intensities of the Cl 2p peaks change with RH while the aerosol mass concentration remains constant. As the RH decreases, the particle signal appears unaffected, while the HCl (g) signal intensifies, indicating that the Cl^- ions are pushed into the gas phase, however, not to an extent that it strongly influences the XPS particle signal. The spectra shown in Figure 3 are not compensated for changes in cross section between particles and photons induced by broadened aerosol beam with decreasing particle size (which is examined in greater detail in Figure 5).

The intensity of the Cl 2p signal from the particle phase and the gas phase cannot be used for absolute quantification purposes. This is because the gas molecule jet, due to the gas molecules high diffusivity, rapidly expands after exiting the aerodynamic lens. The measured HCl (g) signal will therefore depend on how much gas enters through the skimmer separating the ASDS from the GPES, which is strongly influenced by the alignment and the distance between the aerodynamic lens and the skimmer. In contrast, the aerosol particles travel as a collimated and narrow beam after the aerodynamic lens exit, and the signal intensity will not change much by moving the lens closer to the skimmer. Since the position of the aerodynamic lens and the pressure in the GPES remained constant throughout the series of measurements, the HCl (g) signals can be used to identify relative changes in the intensity ratios of the individual spectra, thereby allowing differences in HCl formation to be estimated.

https://doi.org/10.5194/egusphere-2026-6695
Preprint. Discussion started: 5 November 2026
© Author(s) 2026. CC BY 4.0 License.

The formation of HCl is expected to occur when the wet aerosol droplets are dried in the dryers, while no evaporation is expected when they enter the vacuum chamber. To test this hypothesis, a particle filter was placed just before the ASDS entrance to filter out all particles but still letting through the gas (including gaseous HCl). With the particle filter, the doublet associated with the particles disappeared (as expected) while the HCl doublet remained at the same intensity as in the spectrum without particle filter (Figure 4). From this we conclude that the observed HCl formation is not an experimental artifact arising from particles travelling in vacuum. The observation also suggests that losses of HCl (g) in the particle filter are negligible.

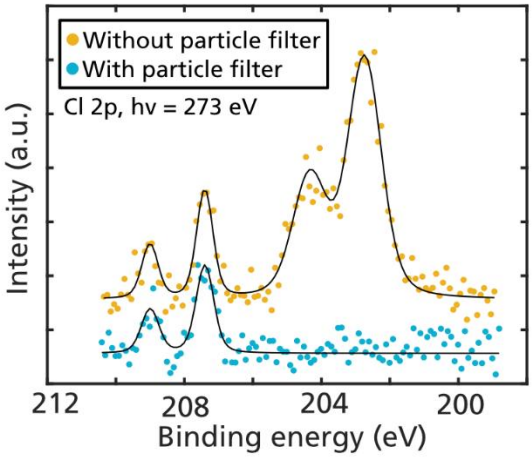


Figure 4: Photoelectron spectra from sampling with particle filter (blue dots) and without particle filter (yellow dots) in front of the ASDS. By adding a particle filter, the doublet at 202-205 eV attributed to Cl in the particles disappears. At the same time the second doublet at 207-210 eV, attributed to HCl gas molecules, remains with similar signal intensity.

Figure 5 shows the intensity of the Cl 2p signal from particles (I_{part}) and from the gaseous HCl (I_{gas}) for different aerosol mass concentrations, as a function of RH. The intensities are obtained from the peak fitting of the Cl 2p spectra, described in detail in previous paragraphs. The signal from the particles (I_{part}) in Figure 5a has been normalized to the total particle surface area concentration derived from the SMPS to account for variations in the total particle surface area over the experiments, due to variations in particle size and number concentration. The XPS signal intensity scales with particle surface area concentration as the surface area determines the effective cross-section exposed to the incident photons. In addition, I_{part} has also been adjusted for size dependent differences in aerosol particle beam broadening between samples occurring after the particles exit the aerodynamic lens. This has been calculated using the aerodynamic lens calculator (Wang and McMurry, 2006), using the surface weighted geometric mean diameter from Figure 2b.

After taking the total particle surface area and the effect of particle beam broadening into consideration, the aerosol mass concentration was shown to have no clear effect on the amount of Cl in the particle phase (Figure 5a). Figure 5b shows the E-AIM modeled aqueous concentration of Cl^- ions in the droplet (C_{part}) as the RH is lowered, taking losses of Cl^- due to the

https://doi.org/10.5194/egusphere-2026-6695
Preprint. Discussion started: 5 November 2026
© Author(s) 2026. CC BY 4.0 License.

formation of HCl into account. The Cl^- concentration is normalized to the initial molar concentration (C_0) of Cl^- to allow a direct comparison between the different ion concentrations. The results in Figure 5b predict a minor concentration dependence on both the aerosol mass concentration and RH in the experimental range used here. At lower mass concentration the Cl^- concentration is slightly decreased when lowering the RH. Yet, the trend is not very strong, as all concentrations are above 88% of the initial concentration. The modeled results support the XPS results, although the small, predicted change cannot be confirmed in the experiments, likely due to experimental uncertainties.

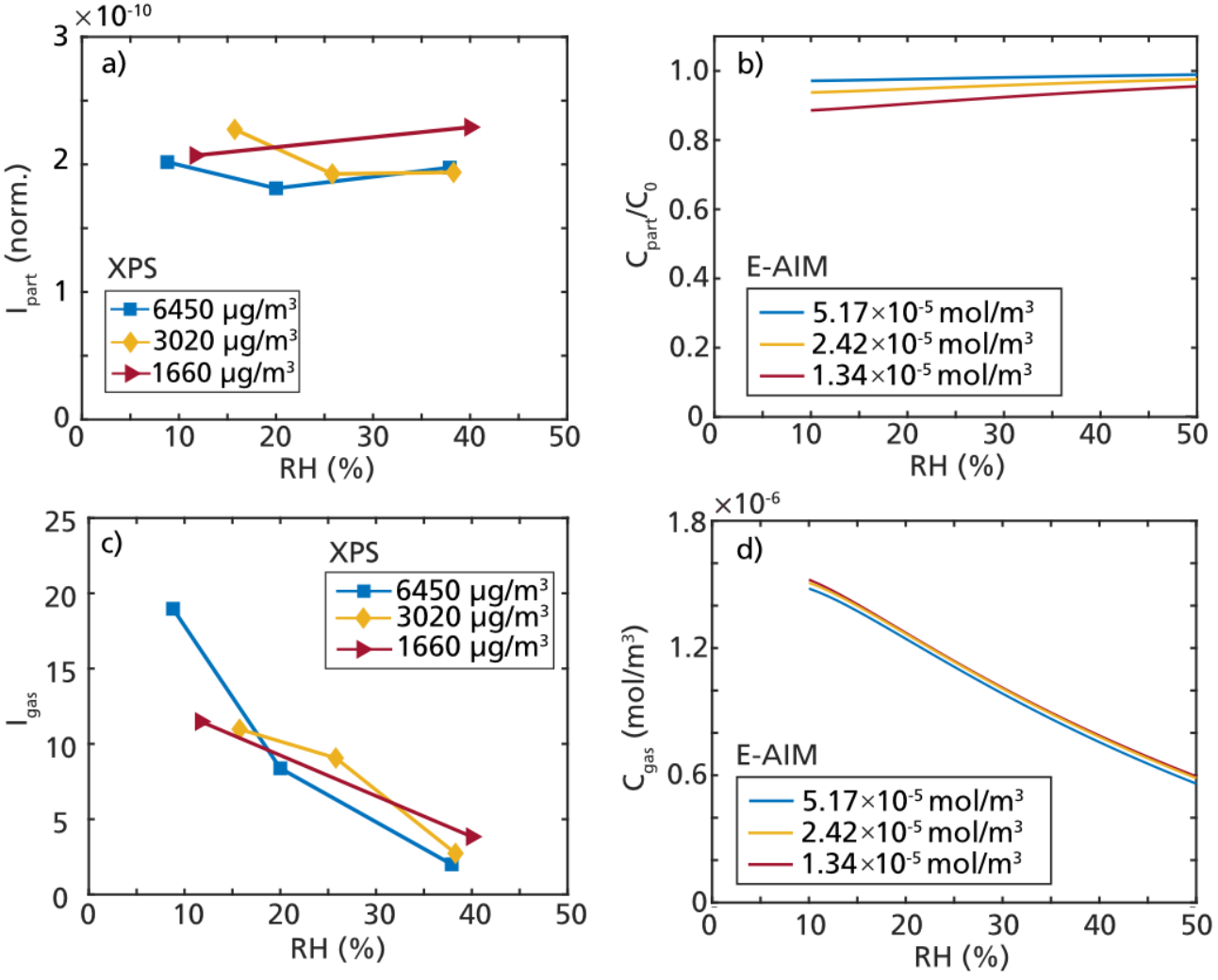


Figure 5: The left panels (a and c) show the variation of the normalized Cl 2p peak area from Cl in the particle phase (a) and gas phase (c) with RH for different aerosol mass concentrations. The right panels (b and d) show the corresponding modeled results by E-AIM. The normalization in (a) has been done with respect to total surface area of the particles and aerosol particle beam broadening.

https://doi.org/10.5194/egusphere-2026-6695
Preprint. Discussion started: 5 November 2026
© Author(s) 2026. CC BY 4.0 License.

In contrast to the almost constant Cl particle signal over RH, the HCl (g) signal measured with XPS shows a strong RH dependence (Figure 5c). At the same time, the signal from the gaseous HCl appears independent of the aerosol mass concentration. The same trend is also predicted by E-AIM modeling at similar concentrations as in the ASDS experiment (C_{gas} in Figure 5d). The increased HCl formation with decreased RH (Figure 5c-d) follows model predictions presented in Rissler et al. (2023). It should be noted that the mass concentrations used in Rissler et al. (2023) were lower (10^{-7} – 10^{-5} mol/m^3) than those used in the current work, which is also the reason why the change in the particle composition of the particles is more pronounced in the earlier study than here. At lower concentrations, HCl formation is expected to exhibit stronger RH dependence, and the relative loss of Cl to the gas-phase is higher. At the higher aerosol mass concentrations used here, the HCl formation still retained RH dependence, but the aerosol mass concentration dependence is weaker. Under these conditions the equilibrium HCl level is reached with only minor relative changes in the particle-phase Cl.

At first, it may seem counterintuitive that the HCl signal increases with decreasing RH while the Cl particle signal remains unchanged. Consider, however, the example of a 100 nm particle shrinking 2 nm due to evaporation of HCl. The 4% reduction in particle surface area will not appreciably change the particle-phase Cl XPS signal but produces a considerable and measurable increase in the gas-phase Cl signal.

The results and trends shown in Figure 5 follow the earlier observations and hypothesis presented by Rissler et al. (2023), where the bulk ratio of ionic compounds was measured using bulk-sensitive aerosol mass spectrometry (AMS) while varying the aerosol mass concentration. Thus, in that earlier study, the evidence of losses of Cl to the gas phase was based on changes observed in the composition of the solid particles, while the HCl (g) was never detected experimentally. Furthermore, that study did not present any experimental proof of the RH dependence of the evaporation although theoretically predicted in the paper. In the current study, the in-flight aerosol XPS method applied enables the detection of gaseous HCl, thereby confirming the mass-dependence effect through simultaneous observations of the distinct XPS signals from Cl in the particle and gas phase.

3.3 Surface components

By analyzing the chemical shifts in the binding energy of Cl photoelectrons emitted from the particles, information about the chemical species formed in the outermost nanometers of the dried particles can be obtained.

In Figure 6a, the Cl 2p photoelectron spectrum from aerosol particles generated from the mixture of NaCl and $(NH_4)_2SO_4$ is compared to those of pure NaCl and NH_4Cl, generated, dried and measured using the same experimental set-up. Due to the difference in the chemical environments of Cl in the two compounds, the measured Cl $2p_{3/2}$ reference binding energy in NaCl (202.87 eV) is higher than in NH_4Cl (202.25 eV).

Figure 6b shows the measured binding energy of Cl at the three aerosol mass concentrations investigated, as a function of RH. In the salt mixture, the Cl $2p_{3/2}$ binding energy of Cl falls between the values observed for pure NH_4Cl and pure NaCl but lies closer to that of NH_4Cl. The binding energy varies with RH, being highest at 40% RH across all three concentrations, whereas

https://doi.org/10.5194/egusphere-2026-6695
Preprint. Discussion started: 5 November 2026
© Author(s) 2026. CC BY 4.0 License.

concentration itself had little effect. This indicates that the surface properties of the aerosol particles are influenced by RH but not by the aerosol mass concentration. Addition of water to NaCl surfaces studied using ambient-pressure X-ray photoelectron spectroscopy (APXPS) has been shown to shift the binding energy towards lower energies in both crystals (Verdaguer et al., 2008) and nanoparticles (Lin et al., 2021) due to surface discharging effects. This effect is not expected to occur in the present study because the aerosol particles are freely suspended and are not in contact with a supporting substrate. Instead, changes in the electronic work function of the aerosol particles associated with changes in surface properties may contribute to the observed binding-energy shifts (Preger et al., 2025).

Another explanation is a change in the surface composition of the particles with RH. For coarse, larger particles, E-AIM modelling predicts that the resulting dried particles are expected to have a mixed composition of $NH_4NaSO_4 \cdot H_2O$, Na_2SO_4, NaCl and NH_4Cl, with NH_4Cl being the dominant component (Tobon et al., 2021). However, resolving the two Cl-containing components in the mixed Cl spectrum is challenging. The energy resolution of the measurements is approximately 500 meV, while the FWHM of the measured Cl peaks is approximately 1.15 eV. Furthermore, the separation between the Cl peaks of the two reference salts is only approximately 0.6 eV. A linear combination of the reference spectra would, in principle, allow the individual contributions from NaCl and NH_4Cl to be attained. However, for reliable confirmation, the spectra would require higher energy resolution to determine whether the observed changes in Cl binding energy with RH arise from changes in the surface composition of the particles or due to shifts in their electronic work function.

Consistent with our findings in the current study, also during the generation and drying of NH_4Cl, HCl is formed (and likely NH_3, although not measured), whereas for NaCl no HCl gas peak could be observed.

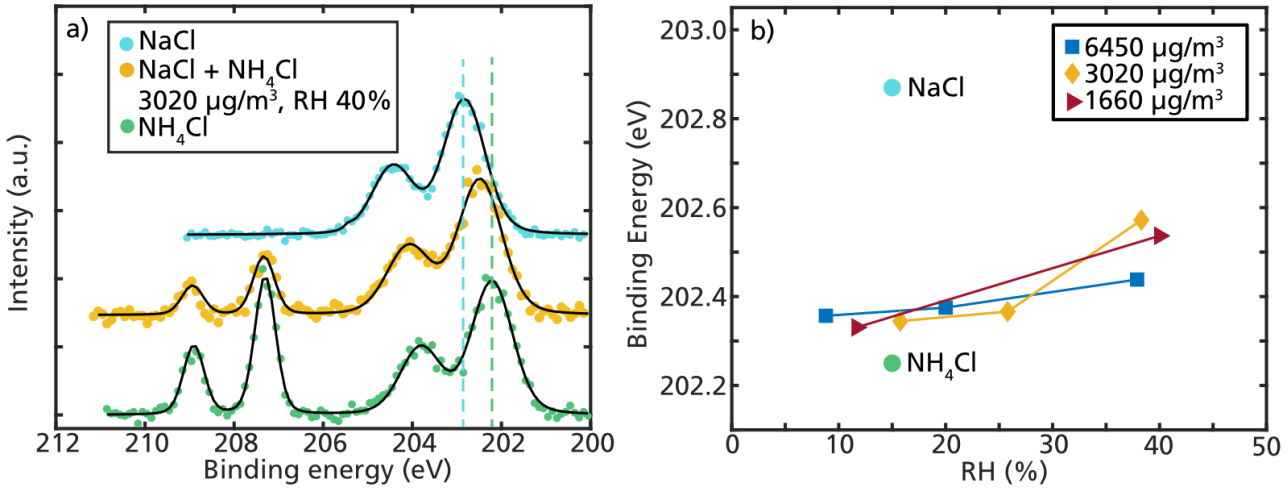


Figure 6: (a) Cl 2p photoelectron spectra of aerosol mixture (yellow dots) and reference aerosol (NaCl, blue dots, and NH_4Cl, green dots). (b) Cl $2p_{3/2}$ (particle) peak binding energy for different aerosol mass concentrations as the RH is changed. Pure NaCl and NH_4Cl measurements are added as references points.

https://doi.org/10.5194/egusphere-2026-6695
Preprint. Discussion started: 5 November 2026
© Author(s) 2026. CC BY 4.0 License.

4. Conclusions

This study confirms the formation of gaseous HCl from aerosols nebulized from a mixed solution of NaCl and $(NH_4)_2SO_4$, by applying in-flight XPS to simultaneously probe particle-phase and gas-phase Cl. By detecting Cl 2p photoelectrons from both the outermost surface of the dry particles and from gaseous HCl, we demonstrate clear formation of gaseous HCl during aerosol generation and drying. Further, this dual-phase measurement enabled investigation of how aerosol mass concentration and RH during drying of nebulized solutions govern the loss of Cl from the particle phase to the gas phase, via the formation of HCl.

We show that there is a strong RH dependent formation of HCl, where the Cl 2p signal from the gas increases when lowering the final RH in the dryer from 40% to 10%. At the same time, in the aerosol mass concentration range investigated, HCl formation is almost independent on the aerosol concentration. In the concentration range investigated here, the predicted differences are small, likely too small to be observed with the current experimental set-up.

In the salt mixture, the binding energy of Cl 2p photoelectrons from the particle phase lies close to that of NH_4Cl, but slightly higher. Furthermore, the binding energy increases with RH. This trend may be caused by changes in surface composition favoring formation of pure NH_4Cl on the particle surfaces at low RH. These results follow the trend in HCl formation, with a dependence of RH, but appear to be independent of the aerosol mass concentration.

The combination of a synchrotron radiation source with an in-flight aerosol sample delivery system enables direct XPS measurement of gas and particle phase compositional changes. Using this approach, we experimentally confirm key aspects of the behavior of laboratory generated NaCl and $(NH_4)_2SO_4$ aerosol mixtures, thereby strengthening the chemical understanding required to accurately predict climate impacts.

Code and data availability

The data that support the findings of this study are publicly available on Zenodo at 10.5281/zenodo.23100469

Author contributions

CP: Writing – Original Draft, Writing – Review & Editing, Visualization, Methodology, Investigation, Formal Analysis, Data Curation, Project Administration. **ACE**: Writing – Review & Editing, Methodology, Investigation, Conceptualization **JJL**: Writing – Review & Editing, Investigation. **NW**: Writing – Review & Editing, Investigation, Funding acquisition. **AK**: Writing – Review & Editing, Investigation. **NLP**: Writing – Review & Editing, Investigation, Funding acquisition, Methodology, Conceptualization **BS**: Writing – Review & Editing, Investigation, Modeling, Conceptualization **JR**: Writing – Original Draft, Writing – Review & Editing, Resources, Methodology, Investigation, Supervision, Project Administration, Conceptualization, Funding Acquisition.

https://doi.org/10.5194/egusphere-2026-6695
Preprint. Discussion started: 5 November 2026
© Author(s) 2026. CC BY 4.0 License.

Competing interests

The authors declare that they have no competing interests

Disclaimer

Copernicus Publications remains neutral with regard to jurisdictional claims made in the text, published maps, institutional affiliations, or any other geographical representation in this paper. While Copernicus Publications makes every effort to include appropriate place names, the final responsibility lies with the authors. Views expressed in the text are those of the authors and do not necessarily reflect the views of the publisher.

Acknowledgements

We acknowledge the MAX IV Laboratory for beamtime on the FinEstBeAMS beamline under (in-house) proposal 20240964. Research conducted at MAX IV, a Swedish national user facility, is supported by Vetenskapsrådet (Swedish Research Council, VR) under contract 2018-07152, Vinnova (Swedish Governmental Agency for Innovation Systems) under contract 2018-04969 and Formas under contract 2019-02496. NLP and JJL gratefully acknowledge the funding from the European Research Council (ERC) under the European Union's Horizon 2020 research and innovation program, project SURFACE (grant agreement no. 717022) and from the Research Council of Finland, including grant nos. 308238, 314175, 335649, 351476, and 361079. BS acknowledge the strategic research area MERGE and Formas. ACE acknowledges support by LINXS Institute of advanced Neutron and X-ray Science.

Review statement

The review statement will be added by Copernicus Publications listing the handling editor as well as all contributing referees according to their status anonymous or identified.

References

Andreae, M. O. and Crutzen, P. J.: Atmospheric aerosols: Biogeochemical sources and role in atmospheric chemistry, Science, 276, 1052–1058, https://doi.org/10.1126/science.276.5315.1052, 1997.

Antonsson, E., Patanen, M., Nicolas, C., Neville, J. J., Benkoula, S., Goel, A., and Miron, C.: Complete Bromide Surface Segregation in Mixed NaCl/NaBr Aerosols Grown from Droplets, Phys. Rev. X, 5, 011025, https://doi.org/10.1103/PhysRevX.5.011025, 2015.

https://doi.org/10.5194/egusphere-2026-6695
Preprint. Discussion started: 5 November 2026
© Author(s) 2026. CC BY 4.0 License.

Barrie, A., Drummond, I. W., and Herd, Q. C.: Correlation of calculated and measured 2p spin-orbit splitting by electron spectroscopy using monochromatic x-radiation, J. Electron Spectros. Relat. Phenomena, 5, 217–225, https://doi.org/10.1016/0368-2048(74)85013-9, 1974.

Calvin, K., Dasgupta, D., Krinner, G., Mukherji, A., Thorne, P. W., Trisos, C., Romero, J., Aldunce, P., Barrett, K., Blanco, G., Cheung, W. W. L., Connors, S., Denton, F., Diongue-Niang, A., Dodman, D., Garschagen, M., Geden, O., Hayward, B., Jones, C., Jotzo, F., Krug, T., Lasco, R., Lee, Y.-Y., Masson-Delmotte, V., Meinshausen, M., Mintenbeck, K., Mokssit, A., Otto, F. E. L., Pathak, M., Pirani, A., Poloczanska, E., Pörtner, H.-O., Revi, A., Roberts, D. C., Roy, J., Ruane, A. C., Skea, J., Shukla, P. R., Slade, R., Slangen, A., Sokona, Y., Sörensson, A. A., Tignor, M., van Vuuren, D., Wei, Y.-M., Winkler, H., Zhai, P., Zommers, Z., Hourcade, J.-C., Johnson, F. X., Pachauri, S., Simpson, N. P., Singh, C., Thomas, A., Totin, E., Alegría, A., Armour, K., Bednar-Friedl, B., Blok, K., Cissé, G., Dentener, F., Eriksen, S., Fischer, E., Garner, G., Guivarch, C., Haasnoot, M., Hansen, G., Hauser, M., Hawkins, E., Hermans, T., Kopp, R., Leprince-Ringuet, N., Lewis, J., Ley, D., Ludden, C., Niamir, L., Nicholls, Z., Some, S., Szopa, S., Trewin, B., van der Wijst, K.-I., Winter, G., Witting, M., Birt, A., and Ha, M.: IPCC, 2023: Climate Change 2023: Synthesis Report. Contribution of Working Groups I, II and III to the Sixth Assessment Report of the Intergovernmental Panel on Climate Change [Core Writing Team, H. Lee and J. Romero (eds.)]. IPCC, Geneva, Switzerland., Geneva, 35–115 pp., https://doi.org/10.59327/IPCC/AR6-9789291691647, 2023.

Chernenko, K., Kivimäki, A., Pärna, R., Wang, W., Sankari, R., Leandersson, M., Tarawneh, H., Pankratov, V., Kook, M., Kukk, E., Reisberg, L., Urpelainen, S., Käämbre, T., Siewert, F., Gwalt, G., Sokolov, A., Lemke, S., Alimov, S., Knedel, J., Kutz, O., Seliger, T., Valden, M., Hirsimäki, M., Kirm, M., and Huttula, M.: Performance and characterization of the FinEstBeAMS beamline at the MAX IV Laboratory, J. Synchrotron Rad., 28, 1–11, https://doi.org/10.1107/s1600577521006032, 2021.

Clegg, S. L., Brimblecombe, P., and Wexler, A. S.: Thermodynamic Model of the System H^+–NH_4^+–Na^+–SO_4^{2-}–NO_3^-–Cl^-–H_2O at 298.15 K, J. Phys. Chem. A, 102, 2155–2171, https://doi.org/10.1021/jp973043j, 1998.

Deal, A. M., Prophet, A. M., Warkander, S., Foreman, M. M., Kim, P., Neumark, D. M., Ahmed, M., and Wilson, K. R.: X-ray photoelectron spectroscopy of surfactants on sub-micron aqueous aerosols, Phys. Chem. Chem. Phys., 27, 17521–17532, https://doi.org/10.1039/d5cp02126j, 2025.

Ellingsen, K., Saue, T., Aksela, H., and Gropen, O.: Cl 2p–photoelectron spectrum of HCl studied by fully relativistic, self-consistent-field, and configuration-interaction calculations, Phys. Rev. A, 55, 2743–2747, https://doi.org/10.1103/PhysRevA.55.2743, 1997.

George, I. J. and Abbatt, J. P. D.: Heterogeneous oxidation of atmospheric aerosol particles by gas-phase radicals, Nat. Chem., 2, 713–722, https://doi.org/10.1038/nchem.806, 2010.

Hallquist, M., Wenger, J. C., Baltensperger, U., Rudich, Y., Simpson, D., Claeys, M., Dommen, J., Donahue, N. M., George, C., Goldstein, A. H., Hamilton, J. F., Herrmann, H., Hoffmann, T., Iinuma, Y., Jang, M., Jenkin, M. E., Jimenez, J. L., Kiendler-Scharr, A., Maenhaut, W., McFiggans, G., Mentel, T. F., Monod, A., Prévôt, A. S. H., Seinfeld, J. H., Surratt, J. D., Szmigielski,

https://doi.org/10.5194/egusphere-2026-6695
Preprint. Discussion started: 5 November 2026
© Author(s) 2026. CC BY 4.0 License.

R., and Wildt, J.: The formation, properties and impact of secondary organic aerosol: current and emerging issues, Atmos. Chem. Phys., 9, 5155–5236, https://doi.org/10.5194/acp-9-5155-2009, 2009.

Goraj, A., Wang, B., Tivanski, A.,and Laskin, A. Hygroscopic Properties of Internally Mixed Particles Composed of NaCl and Water-Soluble Organic Acids, Environ. Sci. Technol., 48(4), 2234-2241, https://doi.org/10.1021/es404727u, 2014

Kivilompolo, M., Kivimäki, A., Jurvansuu, M., Aksela, H., Aksela, S., and Fink, R. F.: The Cl(2p) photoelectron spectra of the HCl and DCl molecules: the effects of the molecular field, J. Phys. B At. Mol. Opt. Phys., 33, L157–L164, https://doi.org/10.1088/0953-4075/33/5/102, 2000.

Kong, X., Fauré, N., Preger, C., Eriksson, A. C., Rissler, J., and Pettersson, J. B. C.: Minor Components in Natural Inorganic Aerosols Dominate Surface Composition: A Contrast Between Surface and Bulk, Environ. Sci. Technol. Lett., 12, 1347–1353, https://doi.org/10.1021/acs.estlett.5c00398, 2025.

Kooser, K., Kivimäki, A., Turunen, P., Pärna, R., Reisberg, L., Kirm, M., Valden, M., Huttula, M., and Kukk, E.: Gas-phase endstation of electron, ion and coincidence spectroscopies for diluted samples at the FinEstBeAMS beamline of the MAX IV 1.5 GeV storage ring, J. Synchrotron Rad., 27, 1080–1091, https://doi.org/10.1107/S1600577520007146, 2020.

Li, W. and Kuwata, M.: Detecting pH of Sub-Micrometer Aerosol Particles Using Fluorescent Probes, Environ. Sci. Technol., 57, 8701–8707, https://doi.org/10.1021/acs.est.3c01517, 2023.

Lin, J. J., Raj R, K., Wang, S., Kokkonen, E., Mikkelä, M. H., Urpelainen, S., and Prisle, N. L.: Pre-deliquescent water uptake in deposited nanoparticles observed with in situ ambient pressure X-ray photoelectron spectroscopy, Atmos. Chem. Phys., 21, 4709–4727, https://doi.org/10.5194/acp-21-4709-2021, 2021.

Liu, P., Ziemann, P. J., Kittelson, D. B., and McMurry, P. H.: Generating particle beams of controlled dimensions and divergence: II. Experimental evaluation of particle motion in aerodynamic lenses and nozzle expansions, Aerosol Sci. Technol., 22, 314–324, https://doi.org/10.1080/02786829408959749, 1995.

Liu, P. S. K., Deng, R., Smith, K. A., Williams, L. R., Jayne, J. T., Canagaratna, M. R., Moore, K., Onasch, T. B., Worsnop, D. R., and Deshler, T.: Transmission efficiency of an aerodynamic focusing lens system: Comparison of model calculations and laboratory measurements for the aerodyne aerosol mass spectrometer, Aerosol Sci. Technol., 41, 721–733, https://doi.org/10.1080/02786820701422278, 2007.

Pelimanni, E., Saak, C. M., Michailoudi, G., Prisle, N., Huttula, M., and Patanen, M.: Solvent and cosolute dependence of Mg surface enrichment in submicron aerosol particles, Phys. Chem. Chem. Phys., 24, 2934–2943, https://doi.org/10.1039/d1cp04953d, 2022.

Preger, C., Rissler, J., Kivimäki, A., Eriksson, A. C., and Walsh, N.: A versatile sample-delivery system for X-ray photoelectron spectroscopy of in-flight aerosols and free nanoparticles at MAX IV Laboratory, J. Synchrotron Rad., 31, 1382–1392, https://doi.org/10.1107/S1600577524005411, 2024.

Preger, C., Jönsson, L., Ternero, P., Sedrpooshan, M., Bermeo, M., Kivimäki, A., Walsh, N., Messing, M. E., Eriksson, A. C., and Rissler, J.: In-Flight Observation and Surface Oxidation Modification of Tin Oxide Nanoparticles for Gas Sensing Applications, ACS Appl. Nano Mater., 8, 6004–6013, https://doi.org/10.1021/acsanm.5c00144, 2025.

https://doi.org/10.5194/egusphere-2026-6695
Preprint. Discussion started: 5 November 2026
© Author(s) 2026. CC BY 4.0 License.

Prisle, N. L.: Surfaces of Atmospheric Droplet Models Probed with Synchrotron XPS on a Liquid Microjet, Acc. Chem. Res., 57, 177–187, https://doi.org/10.1021/acs.accounts.3c00201, 2024.

Prisle, N. L., Engelhart, G. J., Bilde, M., and Donahue, N. M.: Humidity influence on gas-particle phase partitioning of α-pinene + O_3 secondary organic aerosol, Geophys. Res. Lett., 37, 1–5, https://doi.org/10.1029/2009GL041402, 2010.

Ramanathan, V., Crutzen, P. J., Kiehl, J. T., and Rosenfeld, D.: Aerosols, Climate, and the Hydrological Cycle, Science, 294, 2119–2124, https://doi.org/10.1126/science.1064034, 2001.

Rissler, J., Preger, C., Eriksson, A. C., Lin, J. J., Prisle, N. L., and Svenningsson, B.: Missed Evaporation from Atmospherically Relevant Inorganic Mixtures Confounds Experimental Aerosol Studies, Environ. Sci. Technol., 57, 2706–2714, https://doi.org/10.1021/acs.est.2c06545, 2023.

Svenningsson, B., Rissler, J., Swietlicki, E., Mircea, M., Bilde, M., Facchini, M. C., Decesari, S., Fuzzi, S., Zhou, J., Mønster, J., and Rosenørn, T.: Hygroscopic growth and critical supersaturations for mixed aerosol particles of inorganic and organic compounds of atmospheric relevance, Atmos. Chem. Phys., 6, 1937–1952, https://doi.org/10.5194/acp-6-1937-2006, 2006.

Tobon, Y. A., El Hajj, D., Seng, S., Bengrad, F., Moreau, M., Visez, N., Chiapello, I., Crumeyrolle, S., and Choël, M.: Impact of the particle mixing state on the hygroscopicity of internally mixed sodium chloride-ammonium sulfate single droplets: a theoretical and experimental study, Phys. Chem. Chem. Phys., 23, 14391–14403, https://doi.org/10.1039/d1cp01574e, 2021.

Unger, I., Saak, C. M., Salter, M., Zieger, P., Patanen, M., and Björneholm, O.: Influence of Organic Acids on the Surface Composition of Sea Spray Aerosol, J. Phys. Chem. A, 124, 422–429, https://doi.org/10.1021/acs.jpca.9b09710, 2020.

Verdaguer, A., Segura, J. J., Fraxedas, J., Bluhm, H., and Salmeron, M.: Correlation between charge state of insulating NaCl surfaces and ionic mobility induced by water adsorption: A combined ambient pressure X-ray photoelectron spectroscopy and scanning force microscopy study, J. Phys. Chem. C, 112, 16898–16901, https://doi.org/10.1021/jp805444v, 2008.

Wang, X. and McMurry, P. H.: A design tool for aerodynamic lens systems, Aerosol Sci. Technol., 40, 320–334, https://doi.org/10.1080/02786820600615063, 2006.

Zhang, X., Smith, K. A., Worsnop, D. R., Jimenez, J. L., Jayne, J. T., Kolb, C. E., Morris, J., and Davidovits, P.: Numerical characterization of particle beam collimation: Part II integrated aerodynamic-lens-nozzle system, Aerosol Sci. Technol., 38, 619–638, https://doi.org/10.1080/02786820490479833, 2004.

Zieger, P., Väisänen, O., Corbin, J. C., Partridge, D. G., Bastelberger, S., Mousavi-Fard, M., Rosati, B., Gysel, M., Krieger, U. K., Leck, C., Nenes, A., Riipinen, I., Virtanen, A., and Salter, M. E.: Revising the hygroscopicity of inorganic sea salt particles, Nat. Commun., 8, 15883, https://doi.org/10.1038/ncomms15883, 2017.